



 Cite this: *RSC Adv.*, 2022, 12, 27709

## Enhanced antibacterial activity with increasing P doping ratio in CQDs †

 Shuiqin Chai, <sup>\*ab</sup> Lijia Zhou,<sup>b</sup> Yuting Chi,<sup>b</sup> Linshuo Chen, <sup>b</sup> Shuchen Pei <sup>ab</sup> and Bin Chen <sup>\*c</sup>

It is an urgent challenge to develop efficient antibacterial agents against resistant bacteria in the treatment of infectious diseases. Carbon quantum dots (CQDs) have attracted much attention owing to their good stability, low toxicity and excellent biocompatibility. In this work, CQDs doped with different contents of the element phosphorus (P) were prepared by a simple hydrothermal method using valine as a carbon source, triethylamine as a nitrogen source and different volumes of phosphoric acid as a phosphorus source. The average diameter and the surface charge could be regulated from 2.89 nm to 1.56 nm and +2.58 mV to +5.47 mV by increasing the content of the element P in these CQDs. Importantly, these CQDs showed effective bacterial inhibition against *Escherichia coli* (*E. coli*) and *Staphylococcus aureus* (*S. aureus*). The minimal inhibitory concentration (MIC) decreased from 0.71, to 0.51 to 0.18 mg mL<sup>-1</sup> on *E. coli* and *S. aureus* with the increase of P element content. Furthermore, the morphologies of *E. coli* cells and *S. aureus* were damaged and became irregular upon treatment with these CQDs. The results of singlet oxygen (<sup>1</sup>O<sub>2</sub>) detection demonstrated that intracellular <sup>1</sup>O<sub>2</sub> was generated during the antibacterial process. We speculated that bacterial inhibition induced by these CQDs was accompanied by disruption of permeability and structural integrity, owing to strong electrostatic interactions between negatively charged bacteria and positively charged CQDs and production of singlet oxygen of CQDs. Together, this study indicates that the CQDs can be a candidate to treat resistant bacterial infections and may improve the understanding of killing pathogens by antibacterial CQD drugs.

 Received 2nd August 2022  
 Accepted 22nd September 2022

DOI: 10.1039/d2ra04809d

[rsc.li/rsc-advances](https://rsc.li/rsc-advances)

### Introduction

Bacterial infections have been a growing problem worldwide and threaten human life and health.<sup>1</sup> More concerning, super bacteria with superb resistance to antibiotics have risen dramatically due to the abuse of organic antibiotics, increasingly threatening our ability to treat common infections.<sup>2,3</sup> The threat to health of multi-drug resistant bacteria has been extensively reported, suggesting that fatal infections from multi-drug resistant bacteria are predicted to exceed those from cancer by 2050.<sup>4</sup> Thus, it is vital to create new and effective antibacterial agents against resistant bacteria. In the early stage of research, metal nanomaterials, such as gold nanoclusters,<sup>5–7</sup>

silver nanoparticles<sup>8–13</sup> and Cu<sub>2</sub>O nanotubes,<sup>14</sup> have generated a lot of attention due to their significant potential for treating illnesses caused by antibiotic-resistant bacteria. However, the poor environment and biocompatibility of metal nanomaterials has become an obstacle in the clinical application.

As a novel type of carbon nanomaterials, carbon quantum dots (CQDs) with good stability, fluorescence, low toxicity and biocompatibility have been widely used in the fields of bio-imaging, biosensing and drug delivery.<sup>15–24</sup> Additionally, synthetic procedures of CQDs are fairly simple, and the raw materials are cost-efficient and widely available. Thus, CQDs as a new antibacterial agent for biomedical applications have been widely studied.<sup>25–28</sup> Bing *et al.* prepared three kinds of carbon dots with different surface charge, which induced programmed bacteria death.<sup>29</sup> Liu *et al.* used metronidazole to prepare carbon dots with selective antibacterial activity against obligate anaerobes.<sup>30</sup> Furthermore, researchers have performed a series of experiments to explore the antibacterial mechanism of CQDs. For instance, Jian *et al.* proved the cell membranes of *E. coli* and *S. aureus* treated with CQDs for two hours were severely damaged and intact treated without CQDs by TEM and SEM.<sup>31</sup> Lee *et al.* investigated the antibacterial mechanism of CQDs by measuring singlet oxygen (<sup>1</sup>O<sub>2</sub>, a type of ROS) generation using a singlet oxygen sensor green assay, which played an important

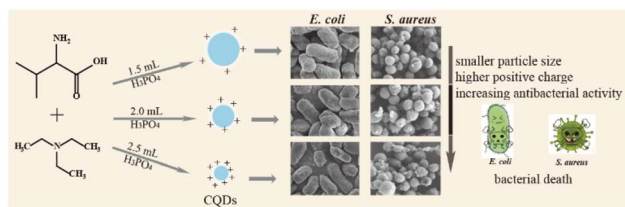
<sup>a</sup>Chongqing Key Laboratory of Industrial Fermentation Microorganism, Chongqing University of Science and Technology, Chongqing 401331, P. R. China. E-mail: chaisq0104@cqust.edu.cn

<sup>b</sup>College of Chemistry and Chemical Engineering, Chongqing University of Science and Technology, Chongqing 401331, P. R. China

<sup>c</sup>Chongqing Key Laboratory of Non-linear Circuit and Intelligent Information Processing, College of Electronic and Information Engineering, Southwest University, Chongqing 400715, P. R. China. E-mail: chenbin121@swu.edu.cn

† Electronic supplementary information (ESI) available: High-resolution XPS spectra of elements; FL emission spectra; stability of CQDs; the antibacterial ability of CQDs. See <https://doi.org/10.1039/d2ra04809d>





**Scheme 1** Schematic illustration of the preparation of CQDs and their antibacterial effects.

role in the eradication of bacteria.<sup>32</sup> The above studies indicate that CQDs destroy bacteria through different mechanisms.

In recent years, the element doping in CQDs has aroused widespread interests of scientists because the doping of elements could effectively adjust some of the available functional groups and chemical properties of prepared CQDs,<sup>33–36</sup> transforming CQDs into functional nanomaterials. For instance, Zhao *et al.* prepared N, P co-doped yellow emitting carbon dots with strong inhibitory ability to bacteria.<sup>37</sup> Travlou *et al.* obtained S- and N-containing CQDs with a capability against Gram-positive and Gram-negative bacterial strains by a simple hydrothermal approach and the N-CQDs exhibited stronger antibacterial ability involved electrostatic interactions.<sup>38</sup>

In this work, we synthesized a series of N, P doped-CQDs using valine as a carbon source, triethylamine as a nitrogen source and different volumes of H<sub>3</sub>PO<sub>4</sub> as a phosphorus (P) source. The functional groups and chemical properties of CQDs were regulated by increasing the content of phosphorus. In addition, these CQDs showed different growth-inhibiting properties by rupturing the cell walls of *E. coli* and *S. aureus*, which might be related to strong electrostatic interactions between negatively charged bacteria and positively charged CQDs and production of <sup>1</sup>O<sub>2</sub> of CQDs, and the antibacterial activity was increased with the increase of P element in the CQDs (Scheme 1).

## Experimental

### Materials

Valine (99%), triethylamine (99%) and 1,3-diphenylisobenzofuran (DPBF) were purchased from Aladdin Reagent Co., Ltd. (Shanghai, China). Sodium chloride, yeast extract, agar powder, tryptone were purchased from Sinopharm Chemical Reagent Co., Ltd. All chemicals were used directly without further purification. All of solutions were prepared with deionized water from a Millipore water purification system (Milli-Q, Millipore, Billerica, USA).

### Apparatus

A RF-5301PC fluorescence spectrophotometer was used to collect all fluorescence spectra (Shimatzu Corp., Kyoto, Japan). Transmission electron microscopy (TEM) and high-resolution transmission electron microscopy (HRTEM) images were collected using a JEOL-2100F transmission electron microscope (Tokyo, Japan). The thickness of P-doped CQDs was carried out

by a Dimension Icon Scan Asyst atomic force microscope (AFM, Bruker Co.). Structural analysis was characterized by D8 ADVANCE X-ray diffraction (XRD, Bruker Co.) using Cu K $\alpha$  radiation ( $\lambda = 0.15406$  nm). Elemental and functional group analyses were measured using an ESCALAB Xi<sup>+</sup> X-ray photoelectron spectrometer (XPS, Thermo Fisher Scientific Inc.) and a Nicolet iS5 Fourier Transform Infrared spectrometer (FTIR, Thermo Fisher Scientific Inc.). Zeta potentials of P-doped CQDs were recorded using a Zetasizer Nano ZS90 System (Malvern, UK). The concentration of bacteria was determined by measuring the optical density at 600 nm (OD<sub>600</sub>) *via* UV-vis spectroscopy. The images of bacteria morphology were obtained under a S-3400N scanning electron microscope (SEM, Hitachi, Japan).

### Synthesis of CQDs

CQDs were prepared *via* a facile one-pot solvothermal method.<sup>39</sup> Briefly, 0.5 g valine, 1 mL triethylamine and different volumes (1.5 mL, 2.0 mL, 2.5 mL) of H<sub>3</sub>PO<sub>4</sub> were dispersed in different volumes (2.5 mL, 2.0 mL, 1.5 mL) of deionized water, respectively. 5.0 mL of the reaction mixture was transferred into a 25 mL poly(tetrafluoroethylene)-lined autoclave, and heated at 180 °C for 12 h, and subsequently cooled to ambient temperature. The solution was filtered using a 0.22  $\mu$ m BIOSHARP membrane filter and dialyzed using a 500 Da dialysis membrane for 48 h. Finally, a series of CQDs powder was obtained by vacuum freeze-drying for 48 h and kept in cold storage at 4 °C. The three CQDs were named by CQDs-1, CQDs-2 and CQDs-3 according to volumes of H<sub>3</sub>PO<sub>4</sub> from 1.5 to 2.5 mL, respectively.

### Cellular toxicity test

$1 \times 10^5$  cells per mL of Human HCT-116 colon cancer cells were seeded on 96-well plates (100  $\mu$ L per well) and grown in McCoy's F-12 cell medium with 10% fetal bovine serum (FBS) at 37 °C. After 24 h, the cells were treated with different doses of CQDs and were incubated with McCoy's F-12 medium with 2% FBS for an additional 24 h. The CQDs-free cells served as control groups. Following the removal of the medium, the cells were washed three times with PBS buffer before being cultured for an additional hour with a mixture of 10  $\mu$ M MTT and 90  $\mu$ L McCoy's F-12 medium. After discarding the MTT culture medium, 150  $\mu$ L of DMSO was added and mixed for around 10 minutes. Finally, the optical density (OD) values of wells were measured at 538 nm. The cell viability was estimated with the eqn (1):

$$\text{Cell viability} = (\text{OD}_{\text{treated}}/\text{OD}_{\text{control}}) \times 100\% \quad (1)$$

where OD<sub>treated</sub> and OD<sub>control</sub> were optical density of cells in the presence and absence of CQDs, respectively.

### Photostability of CQDs

The pH stability was analyzed by mixing 30  $\mu$ L of different pH of Britton–Robinson (BR) buffer with 20  $\mu$ L of CQDs and 450  $\mu$ L deionized water. For ionic strength and oxidation degree, 30  $\mu$ L of various concentrations of NaCl (0–4.0 M) and H<sub>2</sub>O<sub>2</sub> (0–1000  $\mu$ M) solution were mixed with 20  $\mu$ L of CQDs and 30  $\mu$ L PBS

buffer (pH 7.4), and then diluted to 500  $\mu\text{L}$  with deionized water and mixed well. The fluorescence emission of the solutions was observed at a wavelength of 430 nm upon excitation of 320 nm.

### Antibacterial activity test

*S. aureus* and *E. coli* were cultured overnight in lysogeny broth (LB) medium at 37 °C in an orbital shaker (180 rpm). The medium contained 10.0 g of NaCl, 5.0 g of yeast extract powder and 10.0 g of tryptone per liter. Measurements of optical density at 595 nm ( $\text{OD}_{595}$ ) were used to estimate the bacterial concentration. The MIC of CQDs was determined by microdilution with a 96-well cell culture plate. Bacteria were adjusted to  $1.5 \times 10^7$  CFU  $\text{mL}^{-1}$  with LB medium. First, 50  $\mu\text{L}$  of bacterial cell suspension was added to each well. Subsequently, 50  $\mu\text{L}$  of various concentrations of CQDs was dispersed in 96-well plate with a final volume of 100  $\mu\text{L}$  suspension per well and mixed well. Bacteria suspension in an LB medium without CQDs was the control and only LB medium was the blank. The samples were incubated at 37 °C for 12 h with agitation at 180 rpm. After incubation for 12 h, the concentration of bacteria was measured at 595 nm. The experiment was repeated three times.

### Detection of singlet oxygen ( $^1\text{O}_2$ )

The ability of CQDs to generate  $^1\text{O}_2$  under visible light illumination was determined by measuring the absorbance of  $^1\text{O}_2$  quencher 1,3-diphenylisobenzofuran (DPBF) at 410 nm. In present work, an appropriate amount of DPBF and CQDs was added in methanol solution, illuminated upon white LEDs irradiation for 30 min, and the rate of DPBF oxidation was calculated by periodically recording UV-visible spectrum with the absorbance at 410 nm.

## Results and discussion

### Characterizations of the P-doped CQDs

The morphology and structure of the three as-prepared CQDs, noted as CQDs-1, CQDs-2 and CQDs-3, were first characterized by TEM/HRTEM and AFM, respectively. As shown in Fig. 1, the

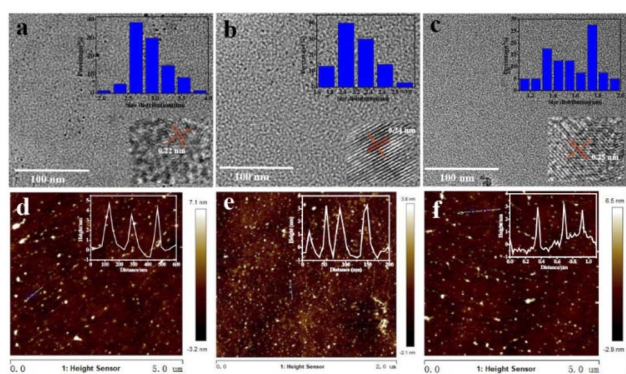


Fig. 1 TEM images of CQDs-1 (a), CQDs-2 (b), and CQDs-3 (c) (inset: the corresponding particle size distribution and HRTEM images) and AFM images of CQDs-1 (d), CQDs-2 (e), and CQDs-3 (f) (inset: the corresponding height profile).

average diameter of CQDs-1, CQDs-2 and CQDs-3 was 2.89 nm, 2.21 nm and 1.56 nm (Fig. 1a–c), respectively. And the average height of CQDs-1, CQDs-2 and CQDs-3 was 4.13 nm, 3.16 nm and 2.93 nm (Fig. 1d–f), respectively. The HRTEM images of these CQDs (inset in Fig. 1a–c) all displayed one in-plane lattice spacings of 0.23 nm which is attributed to the (100) facet of graphene. Furthermore, XRD pattern (Fig. 2a) exhibited a typical broad peak around 22.9° associated with the graphitic structure, further revealing that a typical graphite-like structure is formed during the hydrothermal treatment. The morphology results indicate a declining tendency in size distribution with the increase of the doping ratio of P element from CQDs-1 to CQDs-3.

To investigate the elementary composition and the functional groups in these CQDs, FTIR spectra and XPS were performed. The functional groups on the surface of these CQDs doped with different ratio of P element were characterized by FTIR. As shown in Fig. 2b, the peaks at 3394  $\text{cm}^{-1}$  and 2983  $\text{cm}^{-1}$  were attributed to the stretching vibration of O–H/N–H and C–H,<sup>40,41</sup> the peaks at 1724  $\text{cm}^{-1}$ , 1625  $\text{cm}^{-1}$ , 1472  $\text{cm}^{-1}$  and 1391  $\text{cm}^{-1}$ , 1158  $\text{cm}^{-1}$  were attributed to C=O, C=N, C=C, C–N and C–O stretching vibration,<sup>42,43</sup> the peak at 1002  $\text{cm}^{-1}$  was attributed to P–O stretching vibration.<sup>34,44</sup> As shown in Fig. 3a–c, the full-scan XPS spectra of these CQDs confirmed that all of the CQDs contain four elements involving carbon, nitrogen, oxygen and phosphorus. The elements ratio of C, O, N, P in the three CQDs were 55.43%, 36.86%, 4.39%, 3.32% for CQDs-1 and 33.71%, 57.76%, 3.42%, 5.10% for CQDs-2 and 54.81%, 34.58%, 4.77%, 5.84% for CQDs-3, respectively. Obviously, the doping proportion of P element was increased with the increase of  $\text{H}_3\text{PO}_4$  volumes from CQDs-1 to CQDs-3. As shown in Fig. 3d–f, the high-resolution P 2p spectra of the three CQDs showed two peaks around 134.7 eV and 135.6 eV, which belong to P=O bonds and P=C bonds,<sup>45,46</sup> respectively. As shown in Fig. S1a–c,† the high-resolution C 1s spectra of the three CQDs showed three peaks including 284.8 eV (C=C/C–C bonds), 285.8 eV (C–O/C–N/C–P bonds) and 288.3 eV (C=O bonds).<sup>47</sup> As shown in Fig. S1d–f,† the O 1s spectra of the three CQDs presented two peaks around 532.6 eV (C=O bonds) and 534.5 eV (C–O/P=O bonds).<sup>40</sup> As shown in Fig. S1g–i,† the high-resolution N 1s spectra of the three CQDs revealed the existence of C–N/N–N/P–N bonds (401.0 eV) and N–H bonds (402.8 eV).<sup>45</sup> As demonstrated by the results of FTIR and XPS, the as-prepared three different ratio of P element doped CQDs have abundant

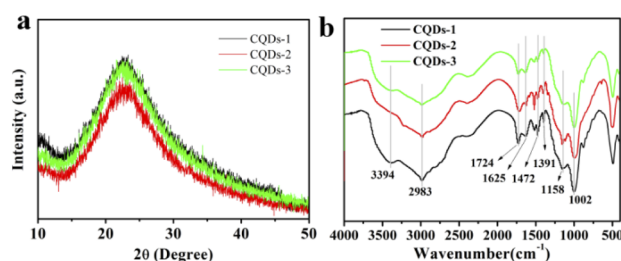


Fig. 2 XRD pattern (a) and FTIR spectra (b) of the as-prepared CQDs-1, CQDs-2 and CQDs-3.

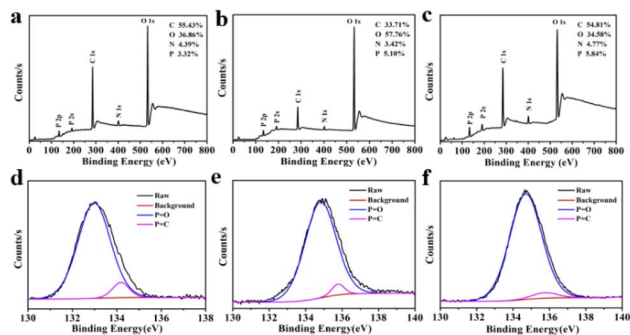


Fig. 3 The full-scan XPS spectra (a–c) the high-resolution P 2p XPS spectra (d–f) of CQDs-1 (a, d), CQDs-2 (b, e) and CQDs-3 (c, f).

functional groups, including –COOH, –OH, and a small number of N, P-containing groups.

### Optical properties of CQDs

As shown in Fig. 4a, the maximum fluorescence (FL) emission was located at 430 nm when excited at 330 nm. While the FL intensity at 430 nm was decreased with the increase of P doping ratio from CQD-1 to CQDs-3. Besides, the maximum emission was independent of the excitation wavelength from 280 nm to 400 nm in these CQDs (Fig. S2†). Fig. 4b showed that all of these CQDs displayed a distinctive absorption peak at 275 nm owing to the  $\pi$ - $\pi^*$  transition of C=C.<sup>48,49</sup> In addition, the as-prepared CQDs showed excellent stability. The FL intensity slightly changed under continuous UV lamp excitation (330 nm) for 60 min, indicating these CQDs have excellent photostability (Fig. S3a†). Meanwhile, the FL intensity almost remained invariant even when the concentrations of NaCl and H<sub>2</sub>O<sub>2</sub> was up to 4 M and 1000  $\mu$ M, respectively, which indicating the stability of these CQDs in comparatively high ionic-strength and oxidation condition (Fig. S3b and c†). These CQDs also showed excellent stability in the pH range from 1.89 to 11.98 (Fig. S3d†).

### Antibacterial activity of CQDs

Before antibacterial activity experiments, we first evaluated the cytotoxicity of these CQDs by MTT method using human HCT-116 colon cancer cells. As depicted in Fig. 5, the cell viability remained greater than 90% after 24 hours of incubation even at concentrations as high as 640  $\mu$ g mL<sup>-1</sup>, indicating that these CQDs have good biocompatibility. Gram-negative *E. coli* and Gram-positive *S. aureus* were used as the model pathogens to

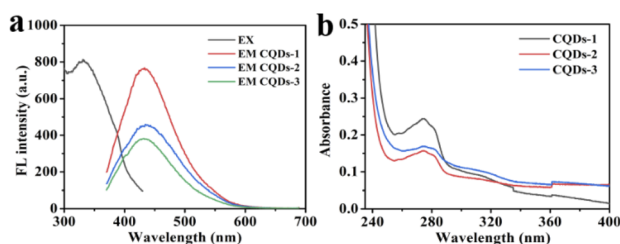


Fig. 4 FL emission spectra (a) and UV-vis absorption (b) of CQDs.

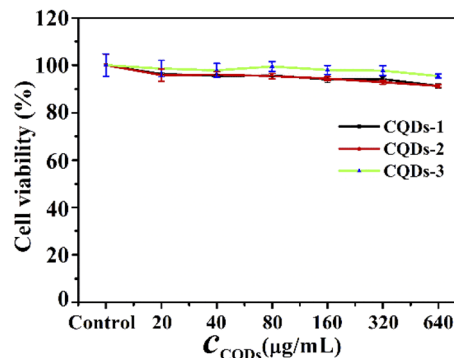


Fig. 5 Cell toxicity of CQDs-1, CQDs-2, CQDs-3 on HCT-116 colon cancer cells.

evaluate the antibacterial activity of these CQDs. Different concentrations of these CQDs were applied to treat equal amounts of bacterial cell suspension for 12 h. The bacterial vitality was evaluated by comparing OD<sub>595</sub> values of the bacterial suspension. As shown in Fig. S4a and d,† the vitality of *E. coli* and *S. aureus* decreased with the increasing concentration of these CQD. The OD<sub>595</sub> of *E. coli* and *S. aureus* were almost consistent with that of the blank group when the concentrations of CQDs-1, CQDs-2, CQDs-3 were respectively up to 0.71, 0.51, 0.18 mg mL<sup>-1</sup>, indicating that these CQDs have not selective inhibitory effect on Gram-negative and Gram-positive pathogens. Besides, to further confirm that these CQDs are not selective for bacteria, we measured the antibacterial activity on *S. flexneri* and *P. aeruginosa* bacteria. As shown in Fig. S4b, c† and Table 1, the MIC values were almost consistent with *E. coli* and *S. aureus*. However, the OD<sub>595</sub> values of *S. aureus* were smaller than that of *E. coli*, *S. flexneri* and *P. aeruginosa* at the same concentration of CQDs, suggesting the inhibitory effect of Gram-positive is stronger than that of Gram-negative pathogens.

In addition, the diameter of the inhibition zone illustrates the bacterial viability of these CQDs. The better the antibacterial ability of CQDs, the larger the diameter of the zone of inhibition. As depicted in Fig. 6, the inhibition diameters of *E. coli* and *S. aureus* became clearly larger with the increase of the doping ratio of P element from CQDs-1 to CQDs-3 and even the inhibition diameter of *S. aureus* was larger than gentamicin (an aminoglycoside antibiotic). The plate colony formation assays of *E. coli* and *S. aureus* treated with these CQDs were shown in Fig. S5.† The results showed that CQDs-3 had the highest antibacterial activity against the tested bacteria, which is consistent with that of the zone of inhibition. These findings

Table 1 The MIC of different CQDs to microorganisms

Bacterial type	MIC (mg mL <sup>-1</sup> )		
	CQDs-1	CQDs-2	CQDs-3
<i>S. aureus</i>	0.71	0.51	0.18
<i>E. coli</i>	0.71	0.51	0.18
<i>S. flexneri</i>	0.71	0.51	0.18
<i>P. aeruginosa</i>	0.71	0.51	0.18

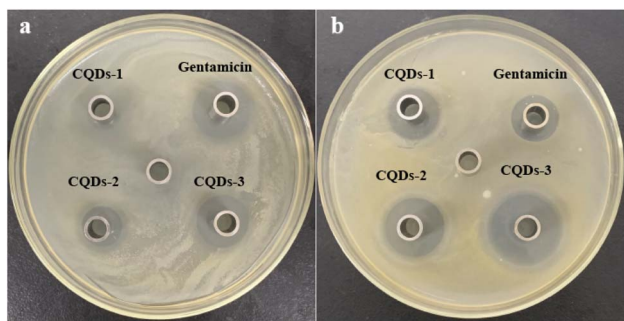


Fig. 6 Photographs of inhibition zone containing *E. coli* (a) and *S. aureus* (b) treated with  $0.71 \text{ mg mL}^{-1}$  of CQDs-1, CQDs-2, CQDs-3 and gentamicin, respectively.

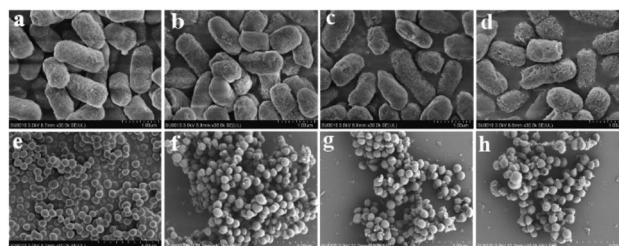


Fig. 8 Bacterial morphology of *E. coli* and *S. aureus* without (a, e) or with CQDs-1 (b, f), CQDs-2 (c, g), CQDs-3 (d, h) treatment.

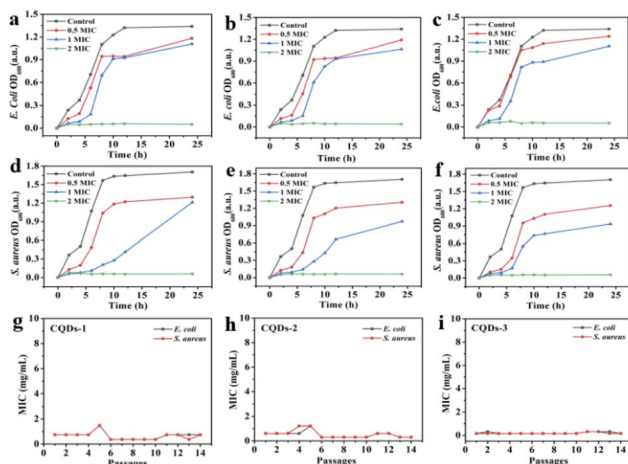


Fig. 7 Inhibition effect of CQDs-1(a, d), CQDs-2 (b, e), CQDs-3 (c, f) on the growth of *E. coli* and *S. aureus*. Drug-resistance study of CQDs-1 (g), CQDs-2 (h), and CQDs-3 (i) against *E. coli* and *S. aureus*.

suggested that the particle size have a certain influence on the antibacterial activity against both *E. coli* and *S. aureus*. Next, the bacterial killing kinetics of these CQDs were studied. Fig. 7a–f showed these CQDs could rapidly eradicate bacteria and displayed a time-dependence at different doses.

To evaluate the potential of bacteria resistance to these CQDs after a continuous antibacterial treatment, bacteria were incubated with half inhibitory concentrations of these CQDs every day and the antibacterial activity was measured through 14 passages. Fig. 7g–i showed the MIC of these CQDs against both *E. coli* and *S. aureus* did not significantly change after 14 passages, indicating that these CQDs have no tendency to develop resistance to *E. coli* and *S. aureus*.

### Antibacterial mechanism of CQDs

To further understand the antibacterial mechanism of these CQDs, the morphologies of bacteria, zeta potential and  $^1\text{O}_2$  production before/after CQDs treatment were studied. As shown in Fig. 8a–h, integrity of *E. coli* and *S. aureus* untreated with CQDs was kept well and smooth while the cell walls of *E. coli* were wrinkled and broken and some cytoplasmic

components of *S. aureus* exudated from cells treated with CQDs, especially in the CQDs-3 groups. In addition, to further investigate the mechanism of antibacterial activity by these CQDs, we explored if  $^1\text{O}_2$  were generated. Fig. 9a–c showed the absorbance feature of DPBF at 410 nm was progressively decreased in the presence of these CQDs, suggesting intracellular singlet oxygen are generated during the antibacterial process. Furthermore, the absorbance of DPBF at 410 nm became lower at 30 min with increasing P element from CQDs-1 to CQDs-3. Meanwhile, the generation of  $^1\text{O}_2$  was further verified by measuring the electron paramagnetic resonance (EPR) of the samples. As shown in Fig. 9d, the signal intensity of  $^1\text{O}_2$  generation increased with the increase of P element. The results are consistent with that of the morphologies of bacteria. As shown in Fig. 10, zeta potential analysis showed that all of CQDs-1 (+2.58 mV), CQDs-2 (+4.33 mV) and CQDs-3 (+5.47 mV) were positively charged, and the positive charge was higher with the doping ratio of P element increased. We speculate that the surface charge of these CQDs is strongly related to antibacterial activity. Overall, these positively charged CQDs destroy the permeability and integrity of the bacterial plasma membrane, maybe owing to the production of reactive oxygen species. Importantly, the CQDs with higher P doping ratio in these carbon nanoparticles, which is smaller in sizes and have higher positive charge, have a significantly enhanced antibacterial activity compared to the others, which may be attributed to the difference in cellular uptake and distribution in the plasma membrane.

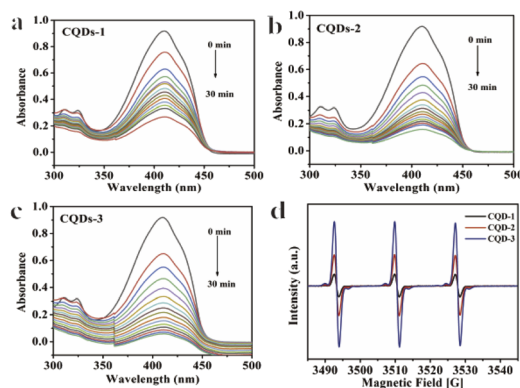


Fig. 9 Absorbance spectra of DPBF obtained from different irradiation times in the presence of CQDs-1 (a), CQDs-2 (b), CQDs-3 (c). EPR spectra (d) of CQDs.

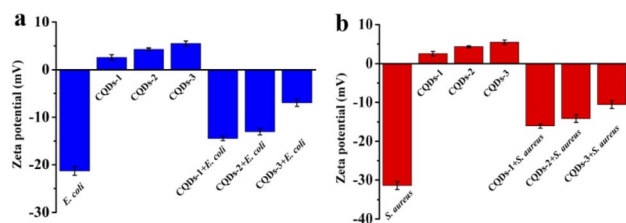


Fig. 10 Zeta potentials of *E. coli*, *S. aureus*, CQDs, *E. coli* + CQDs and *S. aureus* + CQDs.

## Conclusions

In summary, a series of low toxic CQDs with different content of P element were prepared by a hydrothermal method. The average diameter and the surface charge of these CQDs could be regulated by increasing the content of P element. In addition, these positively charged CQDs exhibited effectively enhanced inhibition on Gram-negative and Gram-positive bacteria growth with increasing P doping ratio. The results of antibacterial mechanism demonstrated that bacterial death accompanied by disruption of the permeability and structural integrity of bacterial plasma membrane might be attributed to strong electrostatic interactions between negatively charged bacteria and positively charged CQDs and production of  $^1\text{O}_2$  of CQDs. This work provided a new insight into P-doped CQDs for the development of antibacterial nanomaterials as prospective alternative bacteria-resistant antibacterial agents.

## Author contributions

Data curation, writing-original draft, review, project administration, S. Q. Chai; validation, methodology, formal analysis, L. J. Zhou; formal analysis, investigation, funding acquisition, Y. T. Chi; software, funding acquisition, L. S. Chen; supervision, conceptualization, S. C. Pei; supervision, review and editing, project administration, B. Chen. All authors have read and agreed to the published version of the manuscript.

## Conflicts of interest

There are no conflicts to declare.

## Acknowledgements

This research was funded by Research Foundation of Chongqing University of Science and Technology, grant number ckrc2019031, and Open Fund of Chongqing Key Laboratory of Industrial Fermentation Microorganism (Chongqing University of Science and Technology), grant number GYFJWSW-07, Graduate Innovation Program Project of Chongqing University of Science and Technology, grant number YKJXCX2120532, College Student Innovation Program of Chongqing University of Science and Technology, grant number s202211551015.

## References

- 1 A. Ferreiro, N. Crook, A. J. Gasparrini and G. Dantas, *Cell*, 2018, **172**, 1216–1227.
- 2 M. S. Morehead and C. Scarbrough, *Prim. Care.*, 2018, **45**, 467–484.
- 3 S. B. Singh, K. Young and L. L. Silver, *Biochem. Pharmacol.*, 2017, **133**, 63–73.
- 4 G. F. Zha, H. D. Preetham, S. Rangappa, K. S. Sharath Kumar, Y. R. Girish, K. P. Rakesh, M. Ashrafzadeh, A. Zarrabi and K. S. Rangappa, *Bioorg. Chem.*, 2021, **115**, 105175.
- 5 Y. Z. Y. Xie, W. F. Zheng and X. Y. Jiang, *ACS Appl. Mater. Interfaces*, 2020, **12**, 9041–9049.
- 6 J. C. Kuo, S. H. Tan, Y. C. Hsiao, C. Mutalik, H. M. Chen, S. Yougbaré and T. R. Kuo, *ACS Sustainable Chem. Eng.*, 2022, **10**, 464–471.
- 7 Y. K. Zheng, W. W. Liu, Y. Chen, C. M. Li, H. Jiang and X. M. Wang, *J. Colloid Interface Sci.*, 2019, **546**, 1–10.
- 8 S. Valsalam, P. Agastian, G. A. Esmail, A. K. M. Ghilan, N. A. Al-Dhabi and M. V. Arasu, *J. Photochem. Photobiol., B*, 2019, **201**, 111670.
- 9 M. E. Khan, *Nanoscale Adv.*, 2021, **3**, 1887–1900.
- 10 Z. M. Xiu, Q. B. Zhang, H. L. Puppala, V. L. Colvin and P. J. J. Alvarez, *Nano Lett.*, 2012, **12**, 4271–4275.
- 11 A. Ahmed Sharwani, K. Badri Narayanan, M. Ehtisham Khan and S. Soo Han, *Arab. J. Chem.*, 2021, **14**, 103456.
- 12 M. E. Khan, T. H. Han, M. M. Khan, M. R. Karim and M. H. Cho, *ACS Appl. Nano Mater.*, 2018, **1**, 2912–2922.
- 13 A. A. Sharwani, K. B. Narayanan, M. E. Khan and S. S. Han, *Sci. Rep.*, 2022, **12**, 10017.
- 14 H. Yang, H. Chen, L. Cao, H. Wang, W. F. Deng, Y. M. Tan and Q. J. Xie, *Talanta*, 2020, **212**, 120797.
- 15 Y. Y. Cheng, Y. F. Xie, C. M. Li, Y. F. Li and C. Z. Huang, *Anal. Chem.*, 2019, **91**, 11023–11029.
- 16 Y. Y. Yao, G. Gedda, W. M. Girma, C. L. Yen, Y. C. Ling and J. Y. Chang, *ACS Appl. Mater. Interfaces*, 2017, **9**, 13887–13899.
- 17 M. M. F. Baig and Y. C. Chen, *J. Colloid Interface Sci.*, 2017, **501**, 341–349.
- 18 J. J. Zhao, M. J. Huang, L. L. Zhang, M. B. Zou, D. X. Chen, Y. Huang and S. L. Zhao, *Anal. Chem.*, 2017, **89**, 8044–8049.
- 19 H. P. Liu, T. Ye and C. D. Mao, *Angew. Chem., Int. Ed.*, 2007, **119**, 6593–6595.
- 20 J. Zhou, Y. Yang and C. Y. Zhang, *Chem. Commun.*, 2013, **49**, 8605–8607.
- 21 X. Chu, P. Zhang, Y. Liu, B. Sun, X. Huang, N. Zhou, J. Shen and N. Meng, *J. Mater. Chem. B.*, 2022, **10**, 2865–2874.
- 22 M. E. Khan, A. Mohammad, W. Ali, A. U. Khan, W. Hazmi, W. Zakri and T. Yoon, *J. Cleaner Prod.*, 2022, **349**, 131249.
- 23 M. E. Khan, A. Mohammad and T. Yoon, *Chemosphere*, 2022, **302**, 134815.
- 24 M. Wang, A. Xia, S. Wu and J. Shen, *Langmuir*, 2021, **37**, 7928–7935.
- 25 X. L. Dong, W. X. Liang, M. J. Mezziani, Y. P. Sun and L. J. Yang, *Theranostics*, 2020, **10**, 671–686.

- 26 F. Nichols, J. E. Lu, R. Mercado, M. D. Rojas-Andrade, S. Ning, Z. Azhar, J. Sandhu, R. Cazares, C. Saltikov and S. Chen, *Langmuir*, 2020, **36**, 11629–11636.
- 27 F. C. Cui, Y. L. Ye, J. F. Ping and X. L. Sun, *Biosens. Bioelectron.*, 2020, **156**, 112085.
- 28 A. Anand, B. Unnikrishnan, S. C. Wei, C. P. Chou, L. Z. Zhang and C. C. Huang, *Nanoscale Horiz.*, 2019, **4**, 117–137.
- 29 W. Bing, H. J. Sun, Z. Q. Yan, J. S. Ren and X. G. Qu, *Small*, 2016, **12**, 4713–4718.
- 30 J. J. Liu, S. Y. Lu, Q. L. Tang, K. Zhang, W. X. Yu, H. C. Sun and B. Yang, *Nanoscale*, 2017, **9**, 7135–7142.
- 31 H. J. Jian, R. S. Wu, T. Y. Lin, Y. J. Li, H. J. Lin, S. G. Harroun, J. Y. Lai and C. C. Huang, *ACS Nano*, 2017, **11**, 6703–6716.
- 32 C. H. Lee, S. Y. Song, Y. J. Chung, E. K. Choi, J. Jang, D. H. Lee, H. D. Kim, D.-U. Kim and C. B. Park, *ACS Appl. Bio Mater.*, 2022, **5**, 761–770.
- 33 S. Huang, E. L. Yang, Y. Liu, J. D. Yao, W. Su and Q. Xiao, *Sens. Actuators, B*, 2018, **265**, 326–334.
- 34 B. F. Shi, Y. B. Su, L. L. Zhang, M. J. Huang, R. J. Liu and S. L. Zhao, *ACS Appl. Mater. Interfaces*, 2016, **8**, 10717–10725.
- 35 Z. S. Sun, W. Y. Zhou, J. B. Luo, J. Q. Fan, Z. C. Wu, H. N. Zhu, J. Q. Huang and X. G. Zhang, *J. Colloid Interface Sci.*, 2022, **607**, 16–23.
- 36 M. Wang, Y. Su, Y. Liu, Y. Liang, S. Wu, N. Zhou and J. Shen, *J. Colloid Interface Sci.*, 2022, **608**, 973–983.
- 37 D. Zhao, Z. X. Zhang, X. M. Liu, R. Zhang and X. C. Xiao, *Mater. Sci. Eng. C*, 2021, **119**, 111468.
- 38 N. A. Travlou, D. A. Giannakoudakis, M. Algarra, A. M. Labella, E. Rodríguez-Castellón and T. J. Bandoz, *Carbon*, 2018, **135**, 104–111.
- 39 H. Wang, F. Lu, C. Ma, Y. Ma, M. Zhang, B. Wang, Y. Zhang, Y. Liu, H. Huang and Z. Kang, *J. Mater. Chem. B.*, 2021, **9**, 125–130.
- 40 B. Kong, T. Yang, F. Cheng, Y. Qian, C. Li, L. Zhan, Y. Li, H. Zou and C. Huang, *J. Colloid Interface Sci.*, 2022, **611**, 545–553.
- 41 S. Q. Chai, J. H. He, L. Zhan, Y. F. Li, C. M. Li and C. Z. Huang, *Talanta*, 2019, **196**, 100–108.
- 42 B. Sun, F. Wu, Q. Zhang, X. Chu, Z. Wang, X. Huang, J. Li, C. Yao, N. Zhou and J. Shen, *J. Colloid Interface Sci.*, 2021, **584**, 505–519.
- 43 Y. Q. Zhang, X. Y. Liu, Y. Fan, X. Y. Guo, L. Zhou, Y. Lv and J. Lin, *Nanoscale*, 2016, **8**, 15281–15287.
- 44 M. Algarra, D. Bartolić, K. Radotić, D. Mutavdžić, M. S. Pino-González, E. Rodríguez-Castellón, J. M. Lázaro-Martínez, J. J. Guerrero-González, J. C. G. Esteves da Silva and J. Jiménez-Jiménez, *Talanta*, 2019, **194**, 150–157.
- 45 J. Zhao, F. T. Li, S. Zhang, Y. An and S. Q. Sun, *New J. Chem.*, 2019, **43**, 6332–6342.
- 46 J. Zhou, X. Y. Shan, J. J. Ma, Y. M. Gu, Z. S. Qian, J. R. Chen and H. Feng, *RSC Adv.*, 2014, **4**, 5465–5468.
- 47 H. Wang, F. Lu, C. Ma, Y. Ma, M. Zhang, B. Wang, Y. Zhang, Y. Liu, H. Huang and Z. Kang, *J. Mater. Chem. B.*, 2020, **9**, 125–130.
- 48 J. Xu, Y. Zhou, G. Cheng, M. Dong, S. Liu and C. Huang, *Luminescence*, 2015, **30**, 411–415.
- 49 B. C. M. Martindale, G. A. M. Hutton, C. A. Caputo, S. Prantl, R. Godin, J. R. Durrant and E. Reisner, *Angew. Chem., Int. Ed.*, 2017, **56**, 6459–6463.